ADVANCES IN ATMOSPHERIC SCIENCES, VOL. 42, MAY 2025, 892–903

• **Original Paper** •

# Effect of the Blocking High-East Asian Trough on Three Extreme Cold Events in Eastern Asia

Ziqun ZHANG[1,3,4], Hongyan CUI[*1,3,4], Fangli QIAO[2], Baoxu CHEN[1,3,4], Yang SONG[1], Xiaohui SUN[1,3,4], and Chang GAO[1,3,4]

[1]*College of Mathematics and Physics*, *Qingdao University of Science and Technology*, *Qingdao* 266061, *China*

[2]*The First Institute of Oceanography*, *Ministry of Natural Resources*, *Qingdao* 266061, *China*

[3]*Shandong Engineering Research Center for Marine Scenarized Application of Artificial Intelligence Technology*, *Qingdao* 266061, *China*

[4]*Qingdao Innovation Center of Artificial Intelligence Ocean Technology*, *Qingdao* 266061, *China*

(Received 18 January 2024; revised 19 April 2024; accepted 5 July 2024)

ABSTRACT

Three extreme cold events occurred in eastern Asia in January 2016, January 2021, and December 2023. As important factors in atmospheric circulation anomalies, the Blocking High and East Asian Trough (BH-ET) structure played key roles during these three extreme cold wave events. Among these two dynamic patterns, the BH affected the development of the cold waves in two different ways: (1) before the cold waves in 2016 and 2023, the BH pushed the cold air southward, resulting in a slow and gradual cooling, with a cooling rate (CR) in eastern Asia of 1.34°C $d^{-1}$ and 1.2°C $d^{-1}$, respectively, and (2) in January 2021, the sudden collapse of BH caused the cold air to rapidly attack mid-latitude regions, with a CR of 1.87°C $d^{-1}$. In terms of the spatial CR, the temperature drop in 2021 occurred 38.8 % and 55% faster than those in 2016 and 2023, respectively. At the same time, the ET influences the wind direction of cold waves by modulating the pressure gradient. Before the cold waves occurred, the meridional wind field near the ET showed negative values, forming northwesterly or northeasterly winds, which continued to affect the southern part of East Asia. The meridional wind in January 2021 was stronger than those in 2016 and 2023, which is thought to be the reason for the strength of the 2021 cold wave. Finally, results from the temperature Empirical Orthogonal Function (EOF) analysis from 1980–2023 verify an obvious BH-ET structure in the three cold wave events, which suggests that this particular climatological state provides a climatic background for the occurrence of cold waves.

**Key words:** extreme cold waves, blocking high, East Asian trough, cooling rate

**Citation:** Zhang, Z. Q., H. Y. Cui, F. L. Qiao, B. X. Chen, Y. Song, X. H. Sun, and C. Gao, 2025: Effect of the Blocking High-East Asian Trough on three extreme cold events in Eastern Asia. *Adv. Atmos. Sci.*, **42**(5), 892–903, https://doi.org/10.1007/s00376-024-4029-6.

**Article Highlights:**

- The analysis of the similarities and differences between three typical cold wave weather events that occurred in East Asia is presented.
- The BH-ET structure is one of the contributing factors to the differences in the three cold wave weather events.
- The BH has two forms, among which the collapsible BH causes a sudden cooling for cold waves in eastern Asia.
- The location and intensity of the ET affect the cold wave. The greater the intensity, the more westward its position.

## 1. Introduction

As global warming intensifies, extreme weather has occurred in the Northern Hemisphere with increasing frequency. The Sixth Assessment Report of the Intergovernmental Panel on Climate Change (IPCC AR6) indicates that, as a result of climate change, extreme weather events will become more common in the future. The extreme cold wave is one example of a wintertime extreme weather event. It mainly manifests as a sharp decline in temperature and is often accompanied by strong winds, snowfall, and freezing weather (Park et al., 2010; Song et al., 2019). Weather associated with extreme cold waves has occurred frequently in recent years (Cohen et al., 2020; Vihma et al., 2020; Zhou et al., 2022). Since 2000, extreme cold wave weather has occurred in the winters of 2004/05 (Ding and Ma, 2007), 2007/08 (Zhou et al., 2011), 2009/10 (Hori et al., 2011),

* Corresponding author: Hongyan CUI
Email: cuihy@qust.edu.cn

2015/16 (Ma and Zhu, 2019) and 2020/21 (Zhang et al., 2022a). Among these events, the extreme cold wave during 2015/16 occurred not only in Eurasia but also in North America (Cui and Qiao, 2016; Song et al., 2024). In 2020/21, there were three extreme cold wave events in the Northern Hemisphere, two in Eurasia and one in North America (Zhang et al., 2022b). The frequency and range of cold surges have expanded. Such extreme low-temperature events are considered to occur within a unique temperature pattern known as "Warm Arctic-Cold Eurasia" (Overland et al., 2011), and this pattern has become increasingly obvious in recent years (Cohen et al., 2012; Inoue et al., 2012). Under this pattern, the occurrence of extreme cold wave events is aggravated in the Northern Hemisphere (Jin et al., 2020). In addition, the occurrence of the above-mentioned extreme cold waves is related to an abnormal mid-to-high-latitude large-scale atmospheric circulation, which is connected to the negative phase of the Arctic Oscillation (AO), Ural blocking (Rex, 1950; Kimoto et al., 1992), and the Siberian High (Tao and Wei, 2008; Wen et al., 2009; Zuo et al., 2015). The combination of multiple influential factors is conducive to a more comprehensive analysis of the causes of extreme weather events.

Previous studies have found that the negative phase of the North Atlantic Oscillation (NAO) and blocking cause abnormal mid-to-high-latitude large-scale atmospheric circulations that allow cold Arctic air to invade mid-latitude land areas (Herring et al., 2016; Yao et al., 2016). The effect of the negative phase of NAO is believed to promote the opening of a gap of an otherwise strong, westerly jet, leading to the southward migration of cold polar air (Yao et al., 2016). In addition, blocking plays an important role in the Eurasian extreme cold waves (Luo et al., 2016; Gong and Luo, 2017). Blocking leads to the reduction of sea ice in the Kara and East Siberian Seas, allowing the Arctic vortex to become more unstable, triggering a cold wave through the seasonal accumulation effect (Antokhina et al., 2018; Yao et al., 2022). At the same time, the combination of blocking and the Siberian High enhances the amplitude of the westerly jet and increases the frequency of cold waves over Eurasia (Takaya and Nakamura, 2005; Ma and Zhu, 2019). There is a growing consensus that abnormal atmospheric circulation causes extreme cold wave events (Zheng et al., 2022). However, the effects of blocking and other factors in each extreme weather event differ. Based on such observations, this paper conducts an in-depth analysis. By proposing the Blocking High and East Asian Trough (BH-ET) structure, we analyze the differences between the three extreme cold wave events and point out the roles of this structure. Surface air temperature observations show that the three coldest values in East Asia since 2015 occurred in January 2016, 2021, and December 2023, respectively. Thus, three extreme cold wave weather events that occurred in January 2016, 2021, and December 2023 are selected to analyze the roles of the Blocking High (BH) and East Asian Trough (ET).

The remainder of this paper is organized as follows. The data and methods are introduced in section 2. Section 3 presents the results, including the development process of the three extreme cold weather events, indicators for measuring cooling rate, and the structure of the BH-ET. Conclusions and a final discussion are given in section 4.

## 2. Data and methods

### 2.1. *Datasets*

The daily surface air temperature (SAT) data are from the European Centre for Medium-Range Weather Forecasts reanalysis-5 (ERA5) datasets on a global 0.25°× 0.25° latitude-longitude grid from 2015–23. In addition, the monthly datasets of ERA5 are used to analyze geopotential height (GH), temperature, zonal wind ($U$ wind), and meridional wind ($V$ wind). The spatial resolutions are 0.25° × 0.25°, and the temporal coverage is from 1979–2023. The monthly indices of the NAO and Western Pacific teleconnection (WP) are from the National Oceanic and Atmospheric Administration (NOAA) Climate Prediction Center, obtained from the website of the Climate Indices List.

### 2.2. *Definition of the cold wave events and BH-ET anomalies*

The occurrence process of the extreme cold wave is divided into three stages (Table 1): the outbreak stage, the development stage (the first three days of the outbreak stage continued until before the outbreak stage), and the initial stage (the first 10 days of the development stage continued until before the development stage). Considering the different duration and range of cold wave weather, the outbreak stage of the extreme cold wave is selected by a 5-day moving average. Among them, the outbreak stage has the following characteristics: (1) The 0°C isotherm in the 5-day moving average reaches to the south of North China Plain; (2) The temperature in the Mongolian Plateau and Northeast China is below –20°C; (3) The temperature anomalies across the entirety of East Asia (except the Tibetan Plateau) are negative. This period is defined as a cold wave outbreak stage. In eastern Asia, 20–24 January encompasses the entire outbreak period of the cold surge in 2016, while 4–8 January encompasses the entire outbreak period in 2021. Similarly, the out-

**Table 1**. The stages of cold waves.

| | Jan 2016 | Jan 2021 | Dec 2023 |
|---|---|---|---|
| Initial stage | 7th–17th | 26th (Dec 2020)–1st | 4th–14th |
| Development stage | 17th–19th | 1st–3rd | 14th–16th |
| Outbreak stage | 20th–24th | 4th–8th | 17th–21st |

break period of the extreme cold wave for 2023 occurred from 17–21 December. In the analysis of the atmospheric evolution of these extreme cold waves, anomalies of the 500-hPa geopotential height (GH), surface air temperature (SAT), and U and V-wind fields are used.

In particular, the blocking event over Eurasia is one of the important factors leading to cold waves in Europe and Eastern Asia (Luo et al., 2016; Yao et al., 2016; Li et al., 2020; Kim and Ahn, 2023). It is meaningful to explore the roles of blocking in different events. Yao et al. (2022) pointed out that extreme weather is affected by blocking and that it performs differently in each cold wave event. Here, the blocking discussed is a high-pressure ridge generated in Eastern Europe. Previous studies have two definitions of Ural blocking; one uses a GH anomaly, and the other applies a blocking index (Tibaldi and Molteni, 1990). Among them, the GH anomaly area focuses on the area bounded by (40°–85°N, 30°–150°E). To distinguish between the two structures of BH and ET, two key regions are adjusted on the above-defined regions. One key region for Blocking High (BH) anomalies is defined as the area-averaged 500-hPa GH in the domain bounded by 30°–60°N, 30°–90°E (the blue frame in Fig. 2a). The other, for Eastern Asia Though (ET) anomalies, is defined as the area-averaged 500-hPa GH in the domain bounded by 30°–55°N, 90°–150°E (the red frame in Fig. 2a). Meanwhile, the climatological mean of the GH anomaly field is determined from its mean values during December, January, and February (DJF) from 1979–2023.

### 2.3. *The calculation of cooling rate*

The Cooling Rate (CR) is defined to represent the rate of temperature change, a factor that is directly related to the destructive power of cold surge weather on a spatial scale. The physical meaning of CR is the instantaneous velocity of temperature changes in a certain region. The mathematical expression that defines CR is given by:

$$\mathrm{CR}_{ij} = \frac{1}{\alpha}\lim_{t\to 0}\frac{\Delta \mathrm{Temp}}{\Delta \mathrm{Time}} = \frac{1}{\alpha}\lim_{t\to 0}\frac{\mathrm{Temp}_1 - \mathrm{Temp}_2}{\Delta \mathrm{Time}}, \quad (1)$$

$$\mathrm{CR} = \begin{bmatrix} \mathrm{CR}_{11} & \mathrm{CR}_{12} & \cdots & \mathrm{CR}_{1j} \\ \mathrm{CR}_{21} & \mathrm{CR}_{22} & \cdots & \mathrm{CR}_{2j} \\ \vdots & \vdots & \ddots & \vdots \\ \mathrm{CR}_{i1} & \mathrm{CR}_{i2} & \cdots & \mathrm{CR}_{ij} \end{bmatrix}, \quad (2)$$

where $\mathrm{Temp}_1$ is the temperature before the outbreak of a cold event; $\mathrm{Temp}_2$ is the temperature during the outbreak of a cold event; $t$ represents time; $i, j$ represent latitude and longitude. When $t \to 0$ in the ideal condition, the average velocity approaches the instantaneous velocity. $\alpha$ is the regulating parameter (we set it to $\alpha = 10$ in this paper). Here, the positive and negative values of CR represent different temperature changes. A positive value of CR represents cooling, and a negative value of CR represents warming.

$$\begin{cases} \mathrm{CR}_{ij} \geqslant 0 \iff \text{cool} \\ \mathrm{CR}_{ij} < 0 \iff \text{warm} \end{cases}. \quad (3)$$

By equating the average velocity to the instantaneous velocity at each data point, the model can obtain the instantaneous velocity at multiple points $\mathrm{CR}_{11}$, $\mathrm{CR}_{12}$, ..., $\mathrm{CR}_{ij}$. In this way, a spatial distribution CR for velocity rate of temperature change can be obtained.

### 2.4. *Empirical orthogonal function analysis method*

In this study, the monthly 500-hPa GH and SAT during DJF from 1979–2023 are calculated to examine atmospheric circulation patterns associated with the BH-ET structure in Eastern Asia by the Empirical Orthogonal Function analysis (EOF) method. The monthly SAT and 500-hPa GH anomalies relative to the climatological mean values for 1979–2023 are calculated. Then, the monthly anomalies, weighted according to latitude during DJF from 1979–2023, can obtain the result of spatial modes and the corresponding time series. This method is used to separate the spatial distribution mode of the original temperature field and GH field from the time series. In this paper, the key area for BH is selected by the region (30°–60°N, 30°–90°E), and the key area for ET is selected by the region (30°–55°N, 90°–150°E) according to the result of the EOF. We further note that the spatial distribution mode is only a function of space, and the time series is given in the form of a principal component (PC) value.

## 3. Result

### 3.1. *The three extreme cold weather events in 2016, 2021, and 2023*

In January 2016 and 2021, China experienced two large-scale extreme cold wave weather events. From 20–24 January 2016, a cold wave known as the “Boss” affected most parts of China. During this event Guangzhou, Nanning, and Hong Kong even experienced snowfall. Temperatures in most parts of North China and Mongolia dropped below –20°C. The 0°C isotherm had pushed southward to the central part of South China (Fig. 1a). The temperature anomaly dropped to 8°C–12°C in the Korean Peninsula, Shandong Peninsula, and the southeast coastal area of China, and exceeded –15°C in some places of Northern China (Fig. 1d).

On 4–8 January 2021, an extreme cold wave occurred in the Eastern Asian region, including Mongolia, the Korean Peninsula, Japan, and North China. During this cold wave, the temperature dropped below 0°C over almost all of northern China (Fig. 1b). In particular, more than 60 meteorological stations in eastern and northern China had broken or reached record-low values. For instance, the temperature recorded at Beijing station on 7 January reached –19.6°C, which was its lowest temperature since 1966 (Zhang et al., 2022a). Except for the Tibetan plateau and a few areas in southern China, the temperature anomaly shows that the air temperature decreased in excess of 8°C–10°C (Fig. 1e).

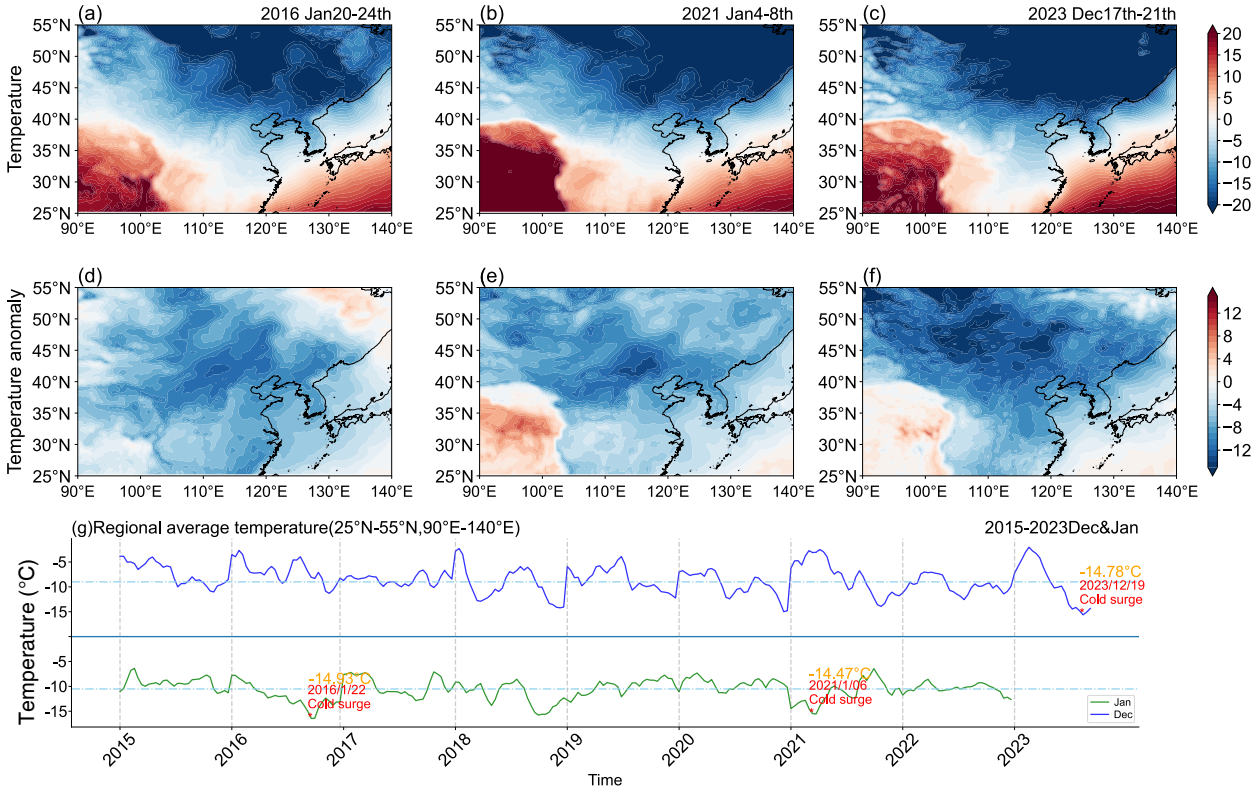


**Fig. 1.** The distribution of SAT and the SAT anomaly (units: °C) during the cold waves of January 2016, January 2021, and December 2023. The (a) SAT and (d) SAT anomaly from 20–24 January 2016. The (b) SAT and (e) SAT anomaly from 4–8 January 2021. The (c) SAT and (f) SAT anomaly from 17–21 December 2023. (g) The daily SAT for December and January from 2015 to 2023.

In December 2023, a cold wave hit the East Asian region, causing severe low temperatures. This extreme cold surge occurred earlier than in previous years. Before the cold wave weather affected southern parts of eastern Asia, extreme cold weather of –40°C occurred in northeastern Inner Mongolia and the northern Heilongjiang Province of China (Fig. 1c). Cold air was pushed to the southern region within a few days, causing the 0°C isotherm to extend to the southern part of Guizhou and the northern part of southern China. The temperature anomaly of this cold wave weather shows that a large area of cooling had occurred in northern East Asia, with a cooling range of –8°C to –12°C, and some areas, i.e., northern Hebei, eastern Inner Mongolia, and Mongolia, the cooling exceeded –12°C (Fig. 1f), and the regional average temperatures dropped to –14.93°C, –14.47°C and –14.78°C, respectively (Fig. 1g, the red points).

### 3.2. *The development process of the three extreme cold weather events*

The East Asian winter cold air activity is closely related to the East Asian winter monsoon system (Qin and Li, 2020). The main components of the system are the Asian subtropical high-latitude westerly jet, the Eurasian mid-to-high latitude blocking high, the East Asian trough, and the Siberian high (Cheung et al., 2012; Zhao et al., 2023). These components reflect the changes in the atmosphere from the bottom, middle, and upper layers of the atmosphere, respectively. Thus, to get a better understanding of the similarities and differences between the three extreme types of cold surge weather, we use the GH, wind anomalies, and SAT to analyze the atmospheric circulation evolution process before the extreme cold surge weather activity (Fig. 2).

In the initial stage of the 2016 event, the SAT in the Arctic rose abnormally, with increases above 5°C–10°C (Fig. 2a), and the polar region was in a warming stage. At this time, the GH in mid-latitude was in a stable state, as the cold air was locked in the polar region. There is a positive SAT anomaly of 6°C–8°C in the key region of the BH. After entering the development stage, a high-pressure ridge appears in the key area of the BH (Fig. 2d). On the west side of the high-pressure ridge, the wind field anomaly enters into the polar region and pours out on the east side. This pushes cold air from Siberia southward. At this moment, the cold air mass in the negative SAT anomaly area stays to the north of eastern Asia. During the outbreak stage, the high-pressure ridge moves eastward and is accompanied by obvious positive SAT anomalies (Fig. 2g). A cyclone is formed over the high-pressure ridge, which drives cold air into the ET and causes extreme cold wave weather.

During the cold wave events in 2021 and 2023, the formation of the BH and the change of the abnormal wind field are consistent with those in 2016, but the role of the BH was different. Based on the performance of different stages, we

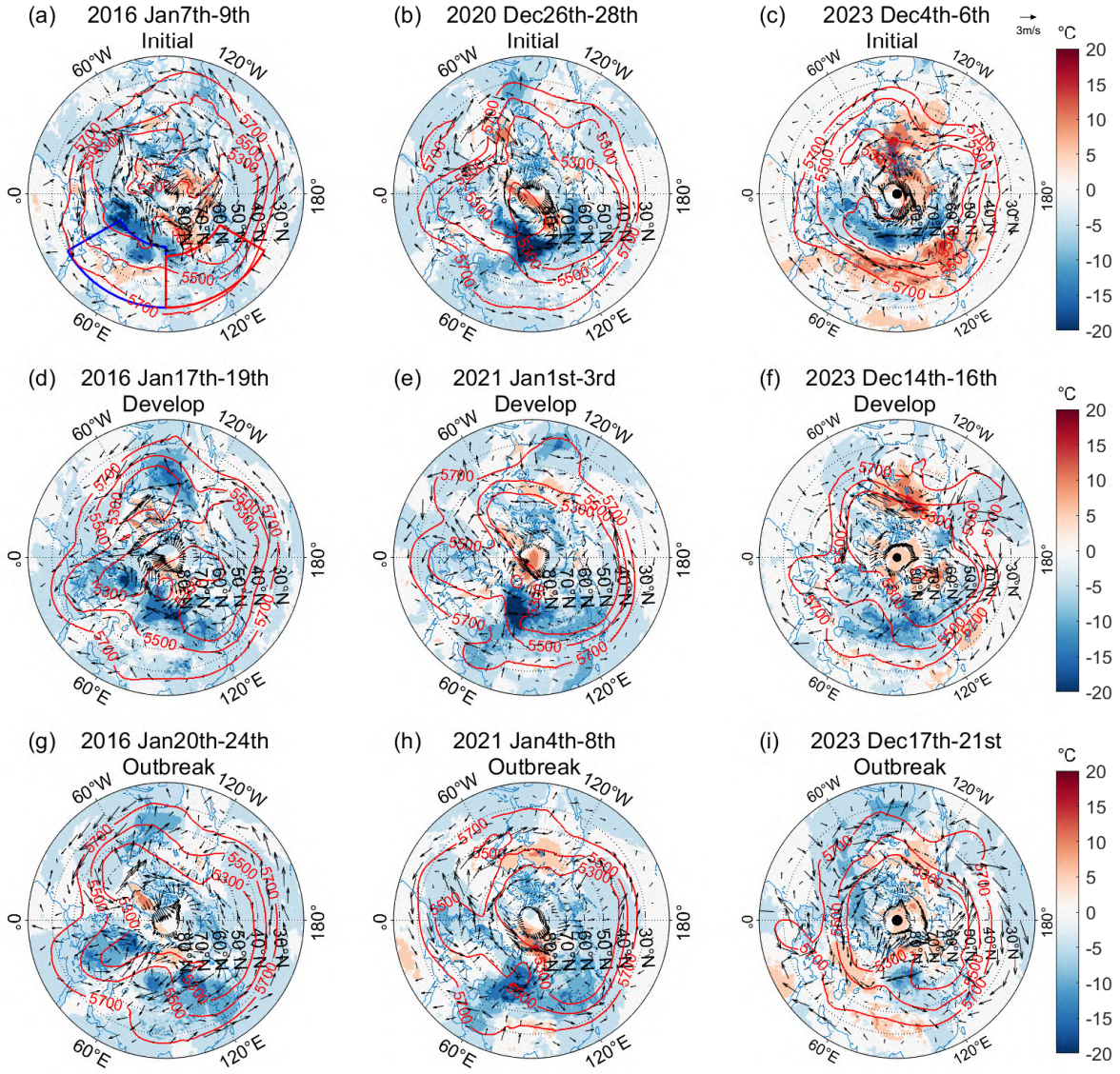


**Fig. 2.** Atmospheric processes related to cold waves: The initial stage of the cold wave is shown for (a) 2016, (b) 2021, and (c) 2023; The development stage is shown for (d) 2016, (e) 2021, and (f) 2023; The outbreak stage is shown for (g) 2016, (h) 2021, and (i) 2023. The red lines represent the 500-hPa GH (units: gpm). The colors denote the SAT anomalies (unit: °C), and the arrows are the wind anomalies (units: m $s^{-1}$).

made the following comparison. In the initial stage of these three cold events, there was a certain degree of positive SAT anomalies in the Arctic. In 2021, it even increased by more than 15°C near the Laptev Sea (Fig. 2b), while the warm anomaly in 2023 was located near the East Siberian Sea and Chukchi Sea (Fig. 2c). The anomalous polar warming is a signal that the southward Arctic cold air is affecting the low latitudes. As evident by the wind anomalies, a large amount of warm air was transported from Eastern Europe to the Arctic by the high-pressure ridge. This was especially true in the Laptev and the Kara Seas, as several cold airflows were pushed to Northern Asia. In the development stage, the BH extends towards the hinterland of Eurasia (Figs. 2d–f). During this stage, a large amount of cold air has already accumulated in the Siberian region. The SAT anomalies show that the temperatures in the Siberian region and the Mongolian Plateau decreased by 10°C–20°C, noting further that the negative SAT anomaly centers were located in Siberia in 2016, the Ural area in 2021, and the Mongolian Plateau in 2023, respectively. These negative SAT anomaly centers can exceed –25°C to –30°C. In the outbreak stage, the BH extends eastward and pushes the cold vortex on the east side of the blocking southward (Figs. 2g, i). Under the stress of the BH, the cold air invades from the northern part of eastern Asia and advances to the south. According to the SAT anomaly, some cold air reaches northern China, causing cooling weather. The anomaly in the Korean Peninsula, the North China Plain, and southern Japan have reached –10°C

to –15°C; the cooling in southern China is even more obvious and reaches –20°C, as the cooling area covers the entirety of eastern Asia. In 2021, the pattern evolved differently; the BH suddenly broke up, allowing the cold air flow to immediately spread to the south (Fig. 2h). In northern China and the Mongolian Plateau, the SAT anomaly reached –20°C and the abnormal center values reached –25°C or more. The negative SAT anomalies caused strong cooling weather in Northern China. Further, there was an area of low pressure over the northern part of eastern Asia, and a cold cyclone appeared over northeast China, which continuously transported cold air southward from Siberia. Due to this characteristic, the cold surge in 2021 was relatively strong, causing pronounced destructive effects by its sudden temperature drops.

In addition to the effects of the BH, the structure of the ET also plays a role in the transport of cold airflow. The ET is considered to be one of the key factors and precursor signals of East Asian low-temperature events caused by strong cold air intrusions (Bueh et al., 2018). The generation of an ET accelerates the airflow from Siberia. In Fig. 3, the longitude-time evolution of the GH and wind fields are calculated during the cold wave.

During the initial period of the cold wave in 2016, the ET gradually formed and expanded westward. Before the development period, between 17–19 January, the low-pressure center appeared east of 120°E (Fig. 3a). Meanwhile, on 17 January 2016, a northwesterly wind developed from 120°E eastward and reached its maximum on the 18th (Figs. 3b, c). Although it weakened slightly during the development period, a stronger northerly wind appeared in northern East Asia, along with the deepening of the ET on the 21st. During the outbreak stage, the *U* and *V*-wind anomalies gradually increased.

The ET intensity during the cold wave period in 2021 was stronger than that in 2016 and 2023 (Fig. 3d). Before the 2021 cold wave, the strong positive *U*-wind anomaly continued from 3 January 2021, reaching its peak value before the outbreak of the cold wave. The maximum *U*-winds were 6.0 m $s^{-1}$ to 11.5 m $s^{-1}$, and the maximum *V*-winds were –7 to –13 m $s^{-1}$ (Figs. 3e, f). The anomalous westward extension of the *U*-wind component was due to the obstruction of the collapse of the atmospheric circulation, which, combined with the atmospheric trough, caused the cold air that initially accumulated in the trough to move suddenly southward. At the same time, the *V*-wind anomaly east of 105°E continued to strengthen during the cold event, providing the force needed for the southward movement of cold air.

During the cold wave event of 2023, the ET structure was not obvious in East Asia until the development period (Fig. 3g). During the period 9–13 December, there was a process in which the positive GH anomaly developed, moved eastward, and then rapidly subsided. The ET then appeared after 15 December, with an intensity 2.9% lower than that of 2021. The westerly winds were much weaker than the previous two events, with weak zonal winds continuing from the 15th (Fig. 3h). By about the 16th, the *V*-wind showed a northerly component moving southeast from around 105°E (Fig. 3i). Affected by the low-pressure trough, cold air was moving southward and affecting the southern region of East Asia. This *V*-wind anomaly was triggered near the East Asian trough, offering further evidence that the East Asian trough plays an important role in the occurrence of cold waves.

Before the outbreak of the cold waves, the *U* and *V*-winds showed a negative anomaly (Figs. 3j, k, yellow box). This is attributed to the fact that the BH-ET structure played an important and proactive role in forcing these anomalies. The appearance of the BH weakened the westerly winds and allowed cold air to enter Siberia. Then, the ET formed, providing for northerly winds to act as a transport mechanism for the cold air to move into eastern Asia. However, cooling does not occur immediately with the change in wind field. It often occurs after the *U*-wind weakens and the *V*-wind strengthens to the south, which allows for extreme cold weather to occur in East Asia, 4–5 days later.

### 3.3. *The indicators for measuring cooling rate*

One of the metrics used to assess extreme cold events is the speed of the temperature change. This is also an important reference indicator for measuring the destructive power of extreme cold wave weather, as a rapid cooling process often leads to more serious consequences. In general, we consider averaging the temperature values in this area to obtain a regional average velocity for temperature change (as shown in the subgraph in Fig. 4). However, the regional average velocity obtained by this method is not accurate because the details at some locations can be averaged out. In the process of understanding extreme weather, we have more stringent requirements on the specific location of cooling. Therefore, we use the local instantaneous velocity matrix CR to describe the rate of temperature change and quantify the speed of temperature change at a given location.

In 2016, the rapidly cooling center in eastern Asia was located in the eastern Tibetan Plateau and the northwest coast of the Japan Sea, with a range of more than 5°C $d^{-1}$–6°C $d^{-1}$, while in most parts of eastern Asia, the CR values are between 2°C $d^{-1}$–3°C $d^{-1}$ (Fig. 4a, the blue lines in subgraph). From the average temperature change in January, the average value during the cold wave outbreak period is 1.34°C $d^{-1}$. In 2021, the rapidly cooling center in Eastern Asia is located to the south of the Mongolian Plateau and North China Plain (Fig. 4b).

The rapid cooling area of the cold wave in 2021 was significantly larger than that in 2016 and was mainly distributed in densely populated areas. The average CR during the cold wave outbreak period is 1.86°C $d^{-1}$. This was 0.52°C $d^{-1}$ faster (an increase of 38.8%) over 2016. In eastern Asia, the CR distribution over the entire region in 2021 tells us that the speed of temperature change was more gentle during the cold wave in 2016. Only along the northern coast of the Sea of Japan and Tibetan Plateau regions, where populations are sparse, were the CR values higher, indicating rapid temperature changes. However, in January 2021, the high CR-value

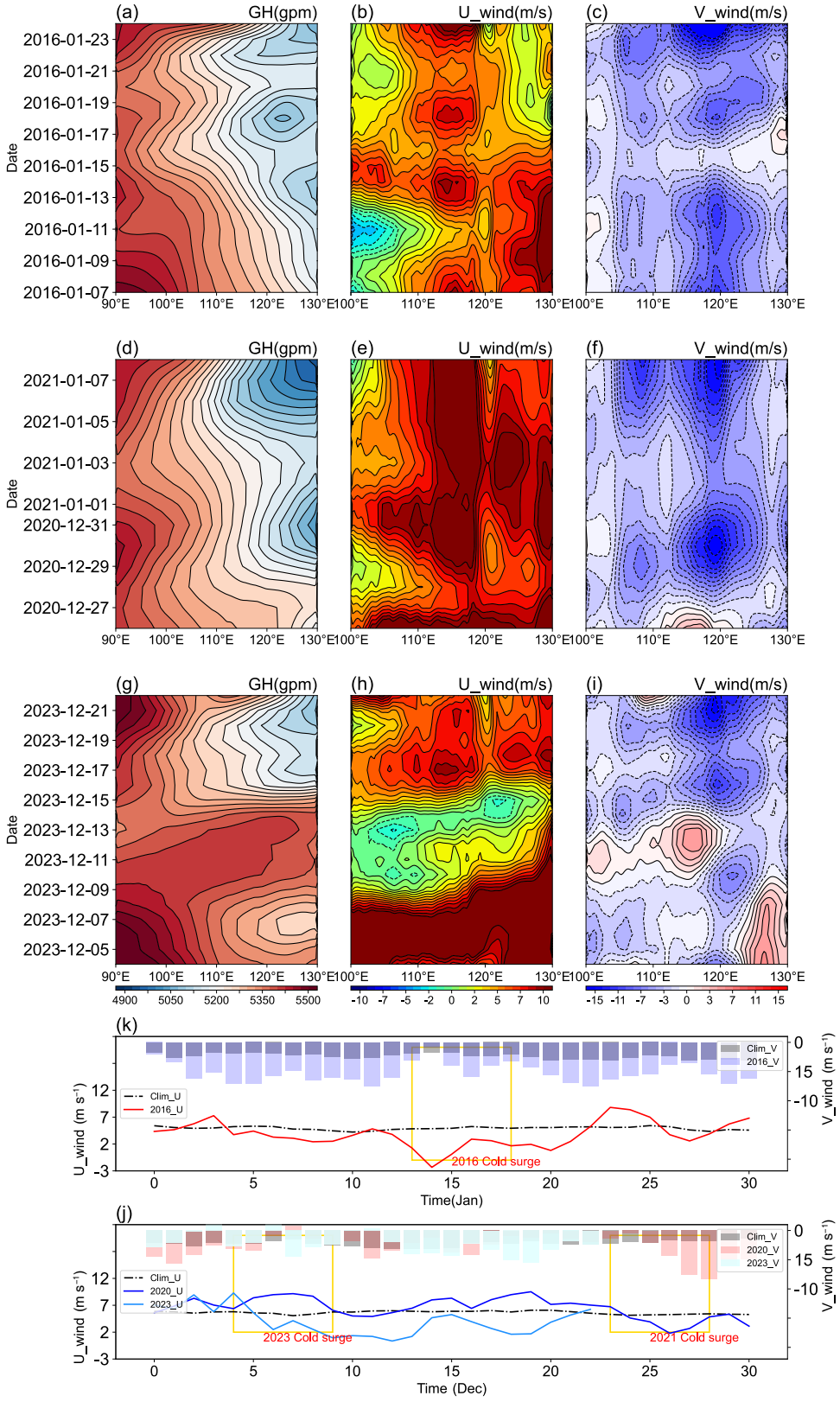


**Fig. 3.** Longitude-time evolution of 40°–60°N for the GH (units: gpm) and *U*/*V* wind (units: m s$^{-1}$) during the cold waves: The January 2016 evolution of the (a) GH, (b) *U*-wind, and (c) *V*-wind; The January 2021 evolution of the (d) GH, (e) *U*-wind, and (f) *V*-wind; the December 2023 evolution of the (g) GH, (h) *U*-wind, and (i) *V*-wind; The daily *U*/*V* wind in (j) December and (k) January (the line represents *U*-wind, and the contours represent the *V*-wind, the black line is the climatology, which is defined as the mean values of 1979–2020).

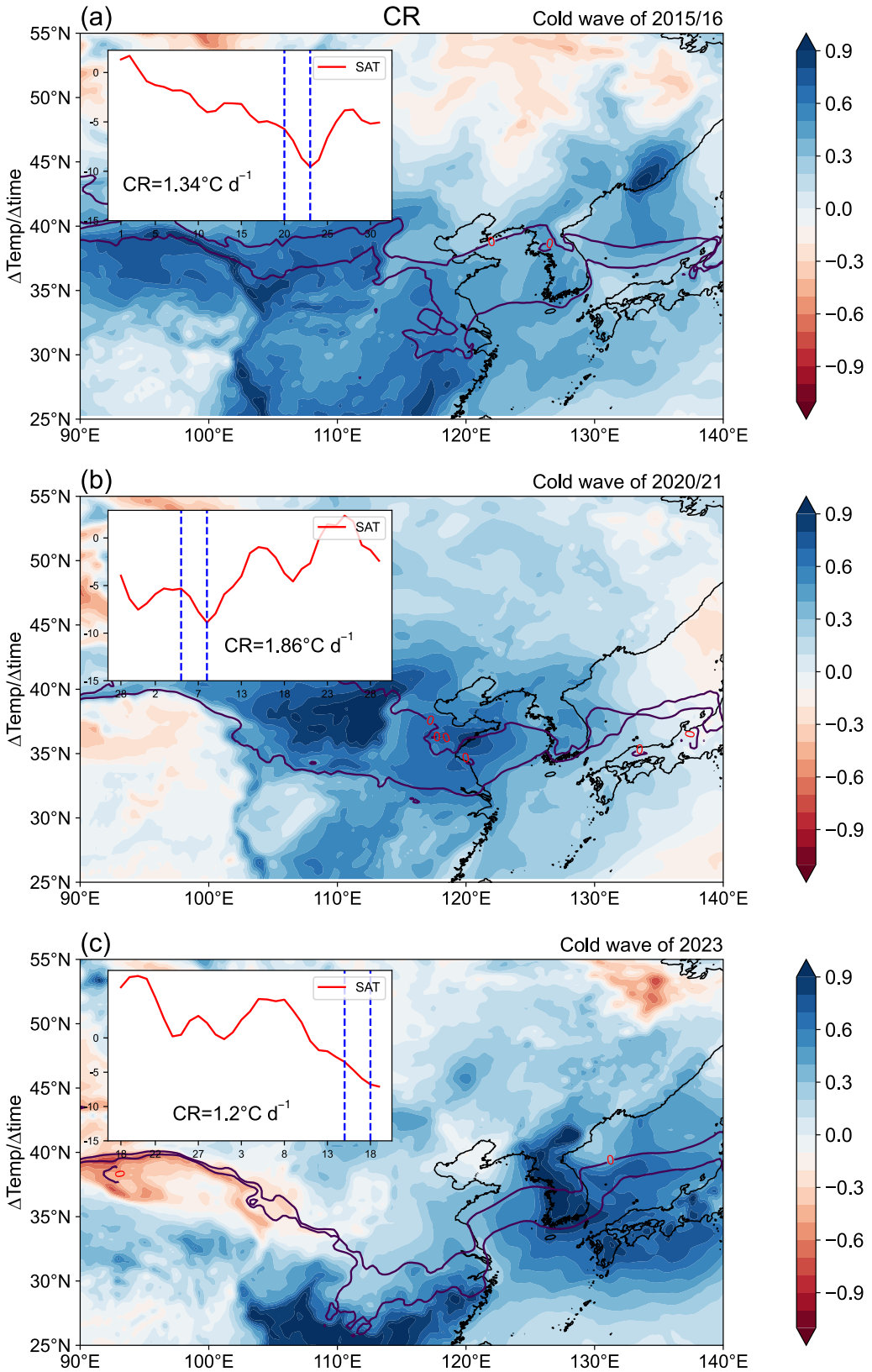


**Fig. 4.** The distribution of cooling rate in Eastern Asia during the extreme cold wave (units: °C d$^{-1}$): (a) The CR in 2016; (b) the CR in 2021; (c) the CR in 2023. The two black lines are the 0°C isotherms; the northern position of the 0°C isotherm was on the first day of the cold wave outbreak, and the southern position was after three days. The red line of the subgraph is the average daily SAT in eastern Asia (25°–55°N, 90°–140°E). The values in the subgraph are the temperature changes between the blue dashed lines.

area was concentrated in the central part of eastern Asia, especially in the North China Plain. Due to its high population density, the rapidly cooling weather in this region had a stronger impact. We also show the location of the 0°C isotherm when these two cold waves occurred (Figs. 4a, b, the black lines). We see that the 0°C isotherm during the cold wave in 2021 is further south than in 2016 during the same stage. This means that the cold air in 2021 moved south faster, and its destructive power was stronger than the slower-moving cold wave in 2016.

The CR in 2023 shows that the low latitudes of southern China and the Korean Peninsula experienced rapid cooling (Fig. 4c). The cooling rate this time was similar to that in 2016, but the impact range was further southward.

### 3.4. *The structure of BH-ET and EOF analysis*

The differences in CR reflect how vigorous the three cold waves were, owing in part to the BH-ET interaction. The analysis of the multi-year anomalies of the BH reveals its indices were 25.24, 20.34, and 8.27 for the cold surges in 2016, 2021, and 2023, respectively, indicating the presence of high pressure in these periods (Fig. 5a). The BH is relatively high before it begins to regulate the movement of cold air in Siberia. Moreover, the BH affects the westerly jet by weakening its intensity, thus increasing the likelihood of triggering instability in the polar vortex (Tyrlis et al., 2019). For the ET anomalies during the three cold waves, the anomalies are –13.9, –22.55, and –30.87 during 2016, 2021, and 2023, respectively (Fig. 5b). Note that the indices of BH anomalies are positive, while the ET indices are negative. Thus, the situation where the BH index is of the opposite sign to that of the ET index is beneficial to the occurrence of extreme cold wave weather. Under this BH-ET structure, the BH mainly affects the westerly wind by pushing and collapsing in such a way that polar cold air enters Siberia. Subsequently, the ET with different intensities and locations serves to transport the cold air into southern East Asia, triggering cold wave weather (Fig. 5c). The BH-ET forms a structure that easily causes the polar cold vortex to become unstable. The high-pressure ridge formed by BH weakens the westerly wind and changes its original path. With the push or collapse of BH, a westerly wind anomaly is triggered, allowing the cold air to be transported southward into the ET. When the position of ET is southerly or westerly, the abnormal strengthening of low pressure causes the occurrence of an East Asian cold wave.

Figure 6 shows the EOF analysis results for GH and SAT in DJF from 1979–2023. In EOF1, there is an obvious

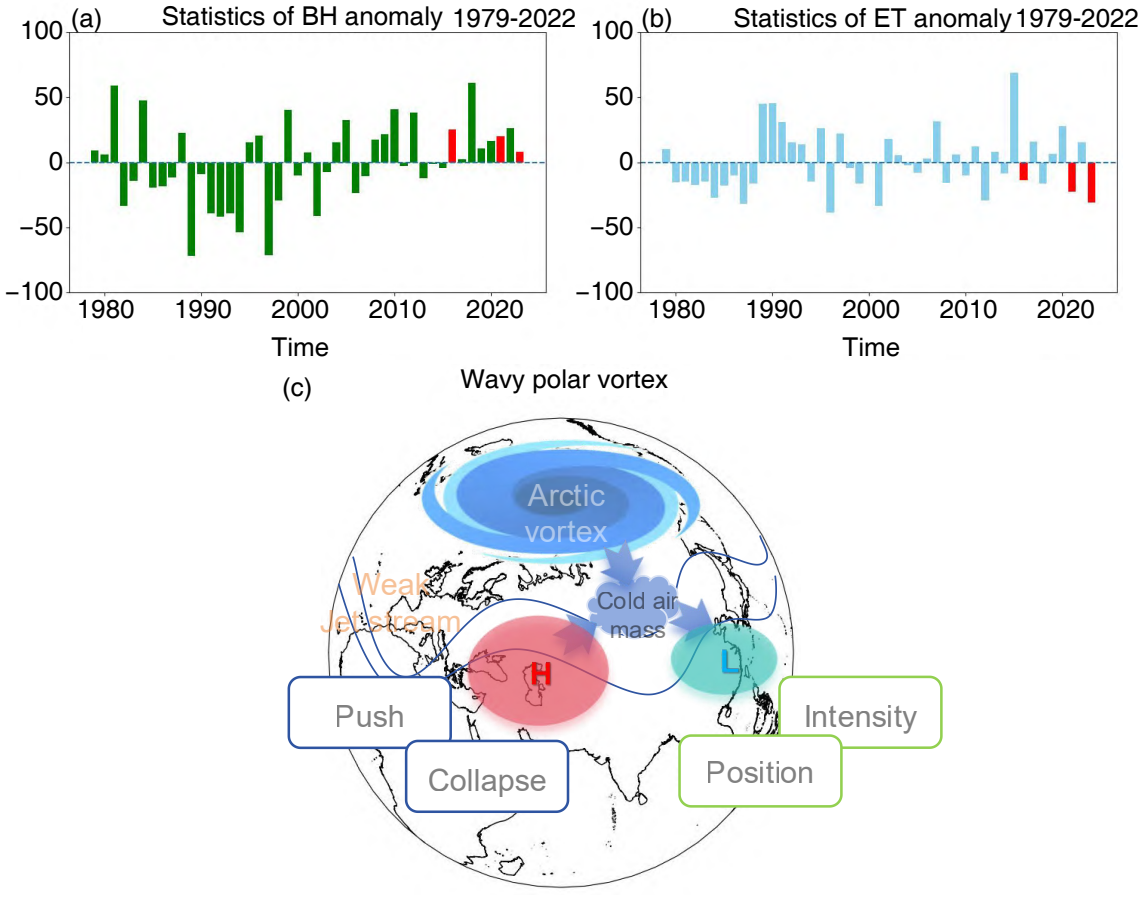


**Fig. 5.** The BH-ET structural diagram and multi-year BH-ET anomalies. The (a) BH and (b) ET anomalies in DJF from 1979–2023 (red bars represent the three cold waves, respectively). (c) The BH-ET structural schematic diagram.

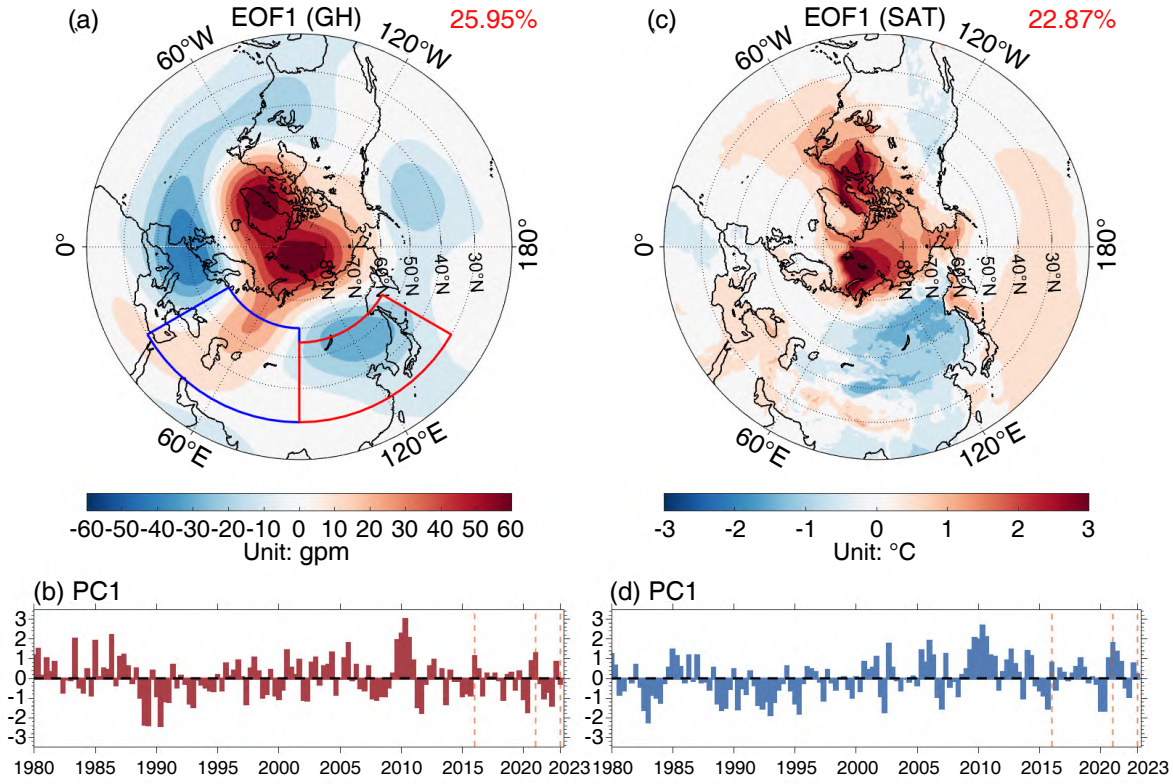


**Fig. 6.** The EOF of GH (units: gpm) and SAT (units: °C): The (a) EOF1 and (b) PC1 of GH during DJF from 1979–2023; the (c) EOF1 and (d) PC1 of SAT. The percentage of variance explained by EOF modes are given in the upper-right corner. The red box represents the key region of the BH. The blue box represents the key region of the ET.

high-pressure structure around 60°E in eastern Europe (Fig. 6a, red box); this mode accounts for 25.95% of the variance. Combined with the PC value (Fig. 6b), it presents a positive pressure anomaly for the winters of 2016, 2021, and 2023. At the same time, there is a low-pressure trough structure at 140°E (Fig. 6a, blue box), with one low-pressure center in the North Pacific Ocean and one in the Sea of Japan. In this mode, the distribution of pressure manifests as a BH-ET structure.

The EOF1 of SAT reflects a "Warm Arctic-Cold Eurasia" pattern, which has been a notable feature for the recent winters in the Northern Hemisphere (Fig. 6c); this mode, mainly manifested in Arctic warming and temperature drops in Siberia (Overland et al., 2011; Cohen et al., 2012), accounts for 22.87% of the variance. The analysis of the EOF1 of SAT and GH suggests that the warming of the Arctic causes the polar pressure gradient to move cold air away from the polar region and transport it into the low-latitude regions of Siberia. This situation was consistent with the climate conditions prior to the three extreme cold waves. Cold air seasonally accumulates in Siberia, and once present, under appropriate conditions, it can be transported to low latitudes, resulting in cooling weather and even extreme cold waves.

## 4. Conclusion and discussion

This study mainly discusses three extreme cold wave events that occurred in eastern Asia in January 2016, January 2021, and December 2023. The roles of the BH-ET structure are analyzed in these cold waves. Meanwhile, the CR is calculated to measure how quickly the temperature dropped in a given region and to determine the destructive effects of the extreme weather. The differences in CR are attributed to the structure of BH-ET for each case.

From the perspective of the structural evolution of the BH, before the cold waves in 2016 and 2023, the BH mainly showed a pushing effect, while in 2021, it showed a blocking collapse. The ET mainly guides the direction of the wind to regulate the transmission of cold air. When cold wave weather occurs, the *V*-wind field shows a negative value, forming a northwest or northeast wind, which continues to affect the southern part of Eastern Asia. The intensity of the ET was different when the three cold waves occurred. The ET in January 2021 was stronger than that in 2016 and 2023, which explains the particular strength of the cold wave in 2021. From the longitude-time evolution, a weakening signal of the *U*-wind appeared in the first 10 days of the development period. During the development period, there was a strong abnormal northerly wind at 120°E. The evolution of such dynamics was caused by the BH-ET structure.

The CR values show that the rates of the cold waves are different. The CR of the cold wave in 2021 was 38.8% and 55% faster than that in 2016 and 2023, respectively, and the impact range of 2021 and 2023 was concentrated in densely

populated areas. Therefore, the destructive power of the cold waves in 2021 and 2023 were higher than that in 2016. From the results of EOF decomposition, the captured BH-ET structure was particularly obvious when the cold waves occurred. The first modes of GH (25.95% of the variance) show an obvious BH-ET structure during the cold waves. This indicates that the BH-ET structure plays an important role in cold-wave weather. The EOF mode of the SAT (22.87% of the variance) shows a cooling trend in East Asia, which is also a background conducive to the occurrence of cold waves.

As an important climate mode in the Northern Hemisphere, the NAO and WP both exert an important impact on the temperature of the Eurasian continent. Zhang et al. (2023) found that when NAO is in its negative phase and the WP is in its positive phase, the northern part of East Asia is cold, and the southern part is warm. Under suitable conditions, the cold air in the north is transported southward, resulting in cooling weather. From the NAO and WP index, the NAO index was –0.37, and the WP index was 0.96 in 2016; in 2021, the NAO index was –1.8, and the WP index was 2.45. These values are in line with this configuration. However, due to its early occurrence, the configuration of the cold wave in 2023 differs from these two events. Therefore, the practicality of solely using the NAO and WP indexes to evaluate early winter cold events in eastern Asia needs to be reconsidered.

***Acknowledgements.*** We thank our colleagues who contributed to drafting the manuscript. The ERA5 Reanalysis data are provided by the ECMWF, from their web site at https://www.ecmwf.int/en/forecasts/datasets/reanalysis-datasets/era5. This research was supported by the National Natural Science Foundation of China under Grant No. 41821004, the National Key Research and Development Program of China under contract No. 2022YFE0140500, the National Key R&D Program of China under contract No. 2022YFA1004403, the Laoshan Laboratory Science and Technology Innovation Project No. LSKJ202202104, the National Nature Science Foundation of China No. 42130406, the Project of Doctoral Found of Qingdao University of Science and Technology under contract No. 2100100 22746.

## REFERENCES

Antokhina, O. Y., P. N. Antokhin, E. V. Devyatova, and Y. V. Martynova, 2018: Atmospheric blockings in Western Siberia. Part 2. Long-term variations in blocking frequency and their relation with climatic variability over Asia. *Russian Meteorology and Hydrology*, **43**, 143–151, https://doi.org/10.3103/S1068373918030020.

Bueh, C., J. B. Peng, Z. W. Xie, and L. R. Ji, 2018: Recent progresses on the studies of wintertime extensive and persistent extreme cold events in China and large-scale tilted ridges and troughs over the Eurasian continent. *Chinese Journal of Atmospheric Sciences*, **42**, 656–676, https://doi.org/10.3878/j.issn.1006-9895.1712.17249.

Cheung, H. N., W. Zhou, H. Y. Mok, and M. C. Wu, 2012: Relationship between Ural-Siberian blocking and the East Asian winter monsoon in relation to the Arctic oscillation and the El Niño-Southern Oscillation. *J. Climate*, **25**, 4242–4257, https://doi.org/10.1175/JCLI-D-11-00225.1.

Cohen, J., and Coauthors, 2020: Divergent consensuses on Arctic amplification influence on midlatitude severe winter weather. *Nature Climate Change*, **10**, 20–29, https://doi.org/10.1038/s41558-019-0662-y.

Cohen, J. L., J. C. Furtado, M. A. Barlow, V. A. Alexeev, and J. E. Cherry, 2012: Arctic warming, increasing snow cover and widespread boreal winter cooling. *Environmental Research Letters*, **7**, 014007, https://doi.org/10.1088/1748-9326/7/1/014007.

Cui, H. Y., and F. L. Qiao, 2016: Analysis of the extremely cold and heavy snowfall in North America in January 2015. *Atmospheric and Oceanic Science Letters*, **9**, 75–82, https://doi.org/10.1080/16742834.2016.1133057.

Ding, Y. H., and X. Q. Ma, 2007: Analysis of isentropic potential vorticity for a strong cold wave in 2004/2005 winter. *Acta Meteorologica Sinica*, **65**, 695–707, https://doi.org/10.11676/qxxb2007.065.

Gong, T. T., and D. H. Luo, 2017: Ural blocking as an amplifier of the Arctic Sea Ice decline in winter. *J. Climate*, **30**, 2639–2654, https://doi.org/10.1175/JCLI-D-16-0548.1.

Herring, S. C., A. Hoell, M. P. Hoerling, J. P. Kossin, C. J. Schreck III, and P. A. Stott, 2016: Introduction to explaining extreme events of 2015 from a climate perspective. *Bull. Amer. Meteor. Soc.*, **97**, S1–S3.

Hori, M. E., J. Inoue, T. Kikuchi, M. Honda, and Y. Tachibana, 2011: Recurrence of intraseasonal cold air outbreak during the 2009/2010 winter in Japan and its ties to the atmospheric condition over the Barents-Kara Sea. *Sola*, **7**, 25–28, https://doi.org/10.2151/sola.2011-007.

Inoue, J., M. E. Hori, and K. Takaya, 2012: The role of Barents Sea ice in the wintertime cyclone track and emergence of a warm-arctic cold-Siberian anomaly. *J. Climate*, **25**, 2561–2568, https://doi.org/10.1175/JCLI-D-11-00449.1.

Jin, C. H., B. Wang, Y.-M. Yang, and J. Liu, 2020: "Warm Arctic-cold Siberia" as an internal mode instigated by North Atlantic warming. *Geophys. Res. Lett.*, **47**, e2019GL086248, https://doi.org/10.1029/2019GL086248.

Kim, E. S., and J. B. Ahn, 2023: Study on the classification and characteristics of cold surge in South Korea. *International Journal of Climatology*, **43**, 720–735, https://doi.org/10.1002/joc.7820.

Kimoto, M., H. Mukougawa, and S. Yoden, 1992: Medium-range forecast skill variation and blocking transition: A case study. *Mon. Wea. Rev.*, **120**(8), 1616–1627, https://doi.org/10.1175/1520-0493(1992)120<1616:MRFSVA>2.0.CO;2.

Li, M. Y., Y. Yao, I. Simmonds, D. H. Luo, L. H. Zhong, and X. D. Chen, 2020: Collaborative impact of the NAO and atmospheric blocking on European heatwaves, with a focus on the hot summer of 2018. *Environmental Research Letters*, **15**, 114003, https://doi.org/10.1088/1748-9326/aba6ad.

Luo, D. H., Y. Q. Xiao, Y. Yao, A. G. Dai, I. Simmonds, and C. L. E. Franzke, 2016: Impact of Ural blocking on winter warm Arctic-cold Eurasian anomalies. Part I: Blocking-induced amplification. *J. Climate*, **29**, 3925–3947, https://doi.org/10.1175/JCLI-D-15-0611.1.

Ma, S. M., and C. W. Zhu, 2019: Extreme cold wave over East Asia in January 2016: A possible response to the larger internal atmospheric variability induced by Arctic warming. *J. Climate*, **32**, 1203–1216, https://doi.org/10.1175/JCLI-D-18-

0234.1.

Overland, J. E., K. R. Wood, and M. Y. Wang, 2011: Warm Arctic-cold continents: Climate impacts of the newly open Arctic Sea. *Polar Research*, **30**, 15787, https://doi.org/10.3402/polar.v30i0.15787.

Park, T.-W., C.-H. Ho, S. Yang, and J.-H. Jeong, 2010: Influences of Arctic Oscillation and Madden-Julian Oscillation on cold surges and heavy snowfalls over Korea: A case study for the winter of 2009–2010. *J. Geophys. Res.: Atmos.*, **115**, D23122, https://doi.org/10.1029/2010JD014794.

Qin, M. Y., and S. L. Li, 2020: Comparison of persistent cold events in China during January-February of 2018 and 2008. *Climatic and Environmental Research*, **25**, 601–615, https://doi.org/10.3878/j.issn.1006-9585.2020.19154.

Rex, D. F., 1950: Blocking action in the middle troposphere and its effect upon regional climate. I: An aerological study of blocking action. *Tellus A*, **2**(3), 196–211, https://doi.org/10.1111/j.2153-3490.1950.tb00331.x.

Song, L., and R. G. Wu, 2019: Different cooperation of the Arctic oscillation and the Madden‐Julian oscillation in the East Asian cold events during early and late winter. *J. Geophys. Res: Atmos.*, **124**, 4913–4931, https://doi.org/10.1029/2019JD030388.

Song, Y., H. Y. Cui, C. S. Xia, B. X. Chen, Z. Q. Zhang, X. H. Sun, and C. Gao, 2024: Analysis of an extreme cold event in North America in December 2022. *Atmosphere*, **15**, 893, https://doi.org/10.3390/atmos15080893.

Takaya, K., and H. Nakamura, 2005: Mechanisms of intraseasonal amplification of the cold Siberian high. *J. Atmos. Sci.*, **62**, 4423–4440, https://doi.org/10.1175/JAS3629.1.

Tao, S.-Y., and J. Wei, 2008: Severe snow and freezing-rain in January 2008 in the southern China. *Climatic and Environmental Research*, **13**, 337–350, https://doi.org/10.3878/j.issn.1006-9585.2008.04.01.

Tibaldi, S., and F. Molteni, 1990: On the operational predictability of blocking. *Tellus A*, **42**, 343–365, https://doi.org/10.3402/tellusa.v42i3.11882.

Tyrlis, E., E. Manzini, J. Bader, J. Ukita, H. Nakamura, and D. Matei, 2019: Ural blocking driving extreme Arctic Sea Ice loss, cold Eurasia, and stratospheric vortex weakening in autumn and early winter 2016–2017. *J. Geophys. Res.: Atmos.*, **124**, 11 313–11 329, https://doi.org/10.1029/2019JD031085.

Vihma, T., and Coauthors, 2020: Effects of the tropospheric large-scale circulation on European winter temperatures during the period of amplified Arctic warming. *International Journal of Climatology*, **40**, 509–529, https://doi.org/10.1002/joc.6225.

Wen, M., S. Yang, A. Kumar, and P. Q. Zhang, 2009: An analysis of the large-scale climate anomalies associated with the snowstorms affecting China in January 2008. *Mon. Wea. Rev.*, **137**, 1111–1131, https://doi.org/10.1175/2008MWR2638.1.

Yao, Y., D. H. Luo, A. G. Dai, and S. B. Feldstein, 2016: The positive North Atlantic oscillation with downstream blocking and middle east snowstorms: Impacts of the North Atlantic jet. *J. Climate*, **29**, 1853–1876, https://doi.org/10.1175/JCLI-D-15-0350.1.

Yao, Y., W. Q. Zhang, D. H. Luo, L. H. Zhong, and L. Pei, 2022: Seasonal cumulative effect of Ural blocking episodes on the frequent cold events in China during the early winter of 2020/21. *Adv. Atmos. Sci.*, **39**, 609–624, https://doi.org/10.1007/s00376-021-1100-4.

Zhang, X. D., Y. F. Fu, Z. Han, J. E. Overland, A. Rinke, H. Tang, T. Vihma, and M. Y. Wang, 2022b: Extreme cold events from East Asia to North America in winter 2020/21: Comparisons, causes, and future implications. *Adv. Atmos. Sci.*, **39**, 553–565, https://doi.org/10.1007/s00376-021-1229-1.

Zhang, Y. X., D. Si, Y. H. Ding, D. B. Jiang, Q. Q. Li, and G. F. Wang, 2022a: Influence of major stratospheric sudden warming on the unprecedented cold wave in East Asia in January 2021. *Adv. Atmos. Sci.*, **39**, 576–590, https://doi.org/10.1007/s00376-022-1318-9.

Zhang, Z. Q., H. Y. Cui, B. X. Chen, H. Cai, and P. Li, 2023: The combined effects of North Atlantic Oscillation and Western Pacific teleconnection on winter temperature in Eastern Asia during 1980–2021. *Acta Oceanologica Sinica*, **42**, 1–9, https://doi.org/10.1007/s13131-023-2187-6.

Zhao, C. B., Q. Q. Li, Y. Nie, F. Wang, B. Xie, L. L. Dong, and J. Wu, 2023: The reversal of surface air temperature anomalies in China between early and late winter 2021/2022: Observations and predictions. *Advances in Climate Change Research*, **14**, 660–670, https://doi.org/10.1016/j.accre.2023.09.004.

Zheng, F., and Coauthors, 2022: The 2020/21 extremely cold winter in china influenced by the synergistic effect of La Niña and warm arctic. *Adv. Atmos. Sci.*, **39**, 546–552, https://doi.org/10.1007/s00376-021-1033-y.

Zhou, B. Z., and Coauthors, 2011: The great 2008 Chinese ice storm: Its socioeconomic-ecological impact and sustainability lessons learned. *Bull. Amer. Meteor. Soc.*, **92**, 47–60, https://doi.org/10.1175/2010BAMS2857.1.

Zhou, T. J., and Coauthors, 2022: 2021: A year of unprecedented climate extremes in Eastern Asia, North America, and Europe. *Adv. Atmos. Sci.*, **39**, 1598–1607, https://doi.org/10.1007/s00376-022-2063-9.

Zuo, Z. Y., R. H. Zhang, Y. Huang, D. Xiao, and D. Guo, 2015: Extreme cold and warm events over China in wintertime. *International Journal of Climatology*, **35**, 3568–3581, https://doi.org/10.1002/joc.4229.